APL Materials

Dirac fermions and possible weak antilocalization in $LaCuSb_2$

Cite as: APL Mater. **7**, 121108 (2019); https://doi.org/10.1063/1.5124685
Submitted: 15 August 2019 . Accepted: 24 November 2019 . Published Online: 16 December 2019

J. R. Chamorro, A. Topp, Y. Fang, M. J. Winiarski, C. R. Ast, M. Krivenkov, A. Varykhalov, B. J. Ramshaw, L. M. Schoop, and T. M. McQueen

Dirac fermions and possible weak antilocalization in $LaCuSb_2$

Cite as: APL Mater. 7, 121108 (2019); doi: 10.1063/1.5124685
Submitted: 15 August 2019 • Accepted: 24 November 2019 •
Published Online: 16 December 2019

J. R. Chamorro,[1,2] A. Topp,[3,4] Y. Fang,[5] M. J. Winiarski,[1,2,6] C. R. Ast,[3] M. Krivenkov,[7] A. Varykhalov,[7] B. J. Ramshaw,[5] L. M. Schoop,[3,4] and T. M. McQueen[1,2,8,a)]

AFFILIATIONS

[1]Department of Chemistry, The Johns Hopkins University, Baltimore, Maryland 21218, USA
[2]Institute for Quantum Matter, Department of Physics and Astronomy, The Johns Hopkins University, Baltimore, Maryland 21218, USA
[3]Max-Planck-Institut für Festkörperforschung, Heisenbergstraβe 1, D-70569 Stuttgart, Germany
[4]Department of Chemistry, Princeton University, Princeton, New Jersey 08544, USA
[5]Laboratory of Atomic and Solid State Physics, Cornell University, Ithaca, New York 14853, USA
[6]Faculty of Applied Physics and Mathematics, Gdansk University of Technology, ul. Narutowicza 11/12, 80-233 Gdansk, Poland
[7]Helmholtz-Zentrum Berlin für Materialien und Energie, Elektronenspeicherring BESSY II, Albert-Einstein-Straße 15, 12489 Berlin, Germany
[8]Department of Materials Science and Engineering, The Johns Hopkins University, Baltimore, Maryland 21218, USA

Note: This paper is part of the Special Topic on Topological Semimetals—New Directions.
[a)]mcqueen@jhu.edu

ABSTRACT

Layered heavy-metal square-lattice compounds have recently emerged as potential Dirac fermion materials due to bonding within those sublattices. We report quantum transport and spectroscopic data on the layered Sb square-lattice material $LaCuSb_2$. Linearly dispersing band crossings, necessary to generate Dirac fermions, are experimentally observed in the electronic band structure observed using angle-resolved photoemission spectroscopy, along with a quasi-two-dimensional Fermi surface. Weak antilocalization that arises from two-dimensional transport is observed in the magnetoresistance, as well as regions of linear dependence, both of which are indicative of topologically nontrivial effects. Measurements of the Shubnikov–de Haas quantum oscillations show low effective mass electrons on the order of $0.065m_e$, further confirming the presence of Dirac fermions in this material.

INTRODUCTION

Topological materials have become very popular over the last decade due to the new and interesting behaviors they display, such as protected edge states, novel excitations, and other unconventional behaviors. There are now many instantiations of topologically nontrivial matter, such as two-dimensional quantum spin Hall phases,[1,2] three-dimensional topological insulators,[3–5] Dirac and Weyl semimetals,[6–8] and nodal line semimetals.[9,10] All of these and more have been the main scope of many theoretical and experimental studies. New materials under these classes present new and exciting possibilities for integration into technology.

Of the many topological classes, Dirac materials present particularly interesting possibilities. In these materials, the energy spectrum of low-energy electrons can be described by using the relativistic Dirac equation, as opposed to the conventional Schrödinger equation. These Dirac fermions can then give rise to a variety of interesting phenomena, such as large, linear magnetoresistances (MRs),[7,11] quantum Hall effects,[12] and high carrier mobilities arising from topological protection.[13,14]

There exist many theoretically and experimentally verified examples of Dirac materials. Aside from the Dirac fermions found on the surfaces of topological insulators, these can also be observed in two-dimensional materials such as graphene[15] or

in bulk three-dimensional Dirac semimetals such as Na_3Bi[6] and Cd_3As_2.[7,11,13] Recently, Dirac fermions have been found in "112" materials with two-dimensional structures, such as layered $AMnSb_2$ and $AMnBi_2$ (A = Ca, Sr, Ba, Eu, Yb)[16–24] and $LaAgSb_2$ and $LaAgBi_2$.[25–27]

The study of Dirac materials often requires a series of complex measurements to establish nontrivial band topology. Their electronic band structures can be calculated using Density Functional Theory (DFT) but often require expensive functionals to ensure a high degree of accuracy. By using angle-resolved photoemission spectroscopy (ARPES), this band structure can be experimentally accessed, which can then be compared to a calculated one for complete understanding. In addition, given the small size of most Dirac Fermi surfaces, these materials display quantum oscillations at relatively low magnetic fields. ARPES and quantum oscillation measurements in conjunction with carrier transport measurements are, therefore, powerful tools to identify the presence of Dirac fermions.

Here, we present ARPES, transport, and quantum oscillation data on $LaCuSb_2$, a tetragonal 112 material with an Sb square lattice. We find two-dimensional weak antilocalization and linear magnetoresistance through transport measurements and confirm the presence of linearly dispersing Dirac bands in the band structure. We observe Shubnikov-de Haas (SdH) oscillations in magnetic fields up to $B = 12$ T and as high as $T = 30$ K and determine a light effective mass of $m^* = 0.065m_e$, as expected for Dirac fermions. Our results demonstrate the presence of Dirac fermions in $LaCuSb_2$.

RESULTS AND DISCUSSION

$LaCuSb_2$ crystallizes in the tetragonal space group $P4/nmm$ (no. 129) and contains alternating layers of a two-dimensional layer of $CuSb_2$ tetrahedra and a two-dimensional Sb square net, separated by La atoms, as shown in Fig. 1(a). It has been reported that variations in Cu content can lead to dramatic changes in the lattice parameters in this material, but our lattice parameters of $a = 4.3828(2)$ and $c = 10.2097(7)$ are consistent[28] with a Cu occupancy of 1.0. In addition, small amounts of excess Sb can be found in all synthesized samples, which is limited to a maximum of 1.5% by mass.

It is the bonding of the Sb atoms in the square net layers that can lead to the formation of linearly dispersing Dirac or Weyl crossings in the electronic band structure due to the symmetry of the Sb p band overlap.[10,29,30] The bandwidth of these linearly dispersing bands is determined by the Sb-Sb interatomic distance, which is 3.08 Å in $LaCuSb_2$. This distance is shorter than in some of the other aforementioned 112 Dirac materials and thus results in linearly dispersive bands with relatively large bandwidths.[16–27] Using a path indicated by the primitive tetragonal Brillouin zone shown in Fig. 1(b), the calculated DFT band structures for $LaCuSb_2$ excluding and including spin-orbit coupling (SOC) are shown in Figs. 1(c) and 1(d), respectively. The two-dimensionality of the structure is reflected in the band structure as the bands become flat and minimally dispersive in reciprocal space directions along k_z, such as Γ–Z and M–A. Dirac fermion behavior may arise as a result of the linearly dispersive bands that cross at certain points in the Brillouin zone, which has also been observed in some of the aforementioned square-net materials. In $LaCuSb_2$, however, there are also several parabolic bands crossing the Fermi level that are primarily Cu-d bands, which may result in some conventional multiband effects. Given that Cu is d^{10} in this system, no magnetism or strong electron correlations are expected.

To further understand the electronic structure of materials, ARPES measurements were performed and compared to DFT calculations. Figure 2(a) shows a constant energy cut at the Fermi level

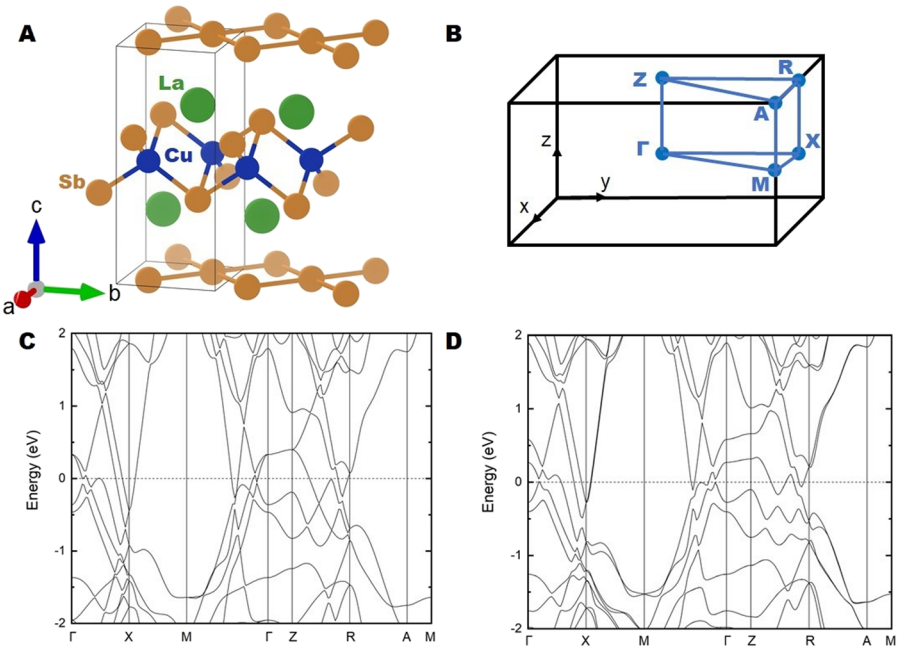

FIG. 1. (a) The tetragonal crystal structure of $LaCuSb_2$, showing the $CuSb_4$ layer and the Sb square-lattice layer. (b) The first Brillouin zone for a primitive tetragonal cell, with special positions highlighted. [(c) and (d)] Show the electronic band structure for $LaCuSb_2$ with and without spin orbit coupling, respectively. Linear bands can be observed especially along X-M and M–Γ with bandwidths on the other of ~1 eV.

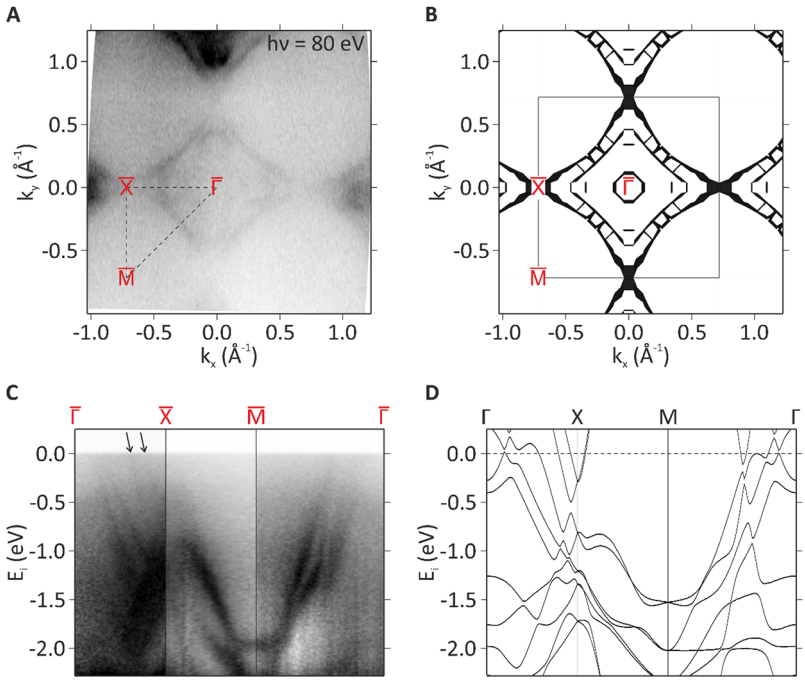

FIG. 2. (a) The experimentally observed Fermi surface measured at $h\nu$ = 80 eV demonstrating a diamondlike shape around the $\overline{\Gamma}$ point. (b) The calculated Fermi surface, which agrees with the experimental one in (a). Internal features are very weak in the first Brillouin zone but are observed in the experimental second Brillouin zone, possibly due to various matrix element effects. (c) The experimentally observed band structure for the $\overline{\Gamma}$–$\overline{X}$–$\overline{M}$–$\overline{\Gamma}$ path along the Brillouin zone. (d) The calculated band structure for the same path as in (c). Deviations observed in the experimental data are likely due to the presence of a small k_z dispersion component (see the supplementary material for comparison).

(E_i = 0 eV) of the first BZ and its vicinity, elucidating the nature of the $LaCuSb_2$ Fermi surface. It consists of a diamondlike feature centered around the $\overline{\Gamma}$ point connected to the next BZ at the $\overline{X}$ points and contains no bands around the $\overline{M}$ point. This kind of diamond-shaped Fermi surface is common for square-net based nodal line materials.[30–32] The literature theoretical value of 0.719 $Å^{-1}$ for the $\overline{\Gamma}$–$\overline{X}$ distance is in accordance with the experimental data.[33] DFT calculations of the Fermi surface, shown in Fig. 2(b), display similar structural behavior but also reveal a cylindrical internal structure inside the diamond centered around $\overline{\Gamma}$, which is weakly visible in the first experimental BZ. Since intensity modulations due to matrix element effects resulting from multiple atoms in the basis affect successive BZs differently, it is also clearly resolved with a higher intensity in neighboring BZs. Figures 2(c) and 2(d) show the experimental and theoretical dispersion plots along the path shown in Fig. 2(b). Both show several bands along $\overline{\Gamma}$–$\overline{X}$, dispersing linearly over a large energy range and crossing the Fermi level (two bands with comparably low intensity are marked with two arrows). To ensure an accurate comparison with the data, one must consider the effect of SOC on the band structure, since the linearly dispersing bands arise from Sb p bands, which can show large avoided crossings due to the large atomic mass of Sb. It should be noted that Fig. 2(d) only shows the $k_z = 0$ plane since it provides the best agreement with the ARPES data (for a comparison with the $k_z = \pi$ plane, see Fig. S1 in the supplementary material).

Since $LaCuSb_2$ is an inversion-symmetric material and time-reversal symmetry is not broken, all bands in the bulk band structure are at least twofold spin degenerate. In addition, the nonsymmorphic symmetry of space group $P4/nmm$ forces additional band degeneracies at the high symmetry points X and M (and R and A, respectively). Along the high-symmetry lines X-M and R-A, however, the degeneracy is not protected by nonsymmorphic symmetry in the presence of SOC, although the splitting of the bands appears to be quite weak and proves difficult to resolve in the experimental data. Deviations between the experimentally observed bands and the presented DFT calculations can be explained by a small change of k_z throughout the BZ and a small offset from the high-symmetry plane $k_z = 0$ for the presented constant photon energy of 80 eV. Overall, however, the experimental band dispersions are in good agreement with the DFT calculations, confirming the presence of linearly dispersing bands belonging to Dirac crossings that can give rise to Dirac fermions in $LaCuSb_2$.

Transport measurements of $LaCuSb_2$ provide insight into its electronic behavior. The resistivity of $LaCuSb_2$ at room temperature amounts to 1.3 mΩ cm. The resistivity decreases with temperature, as expected for a metal, and generally increases with the applied magnetic field, as shown in Fig. 3(a). The residual resistivity ratio (RRR) is 8.5, as given by ρ_{250K}/ρ_{3K}, and is indicative of a high-quality crystal. The magnetoresistance (MR) of $LaCuSb_2$, however, shows more interesting behavior. At low magnetic fields and low temperatures, the MR defined as $(\rho(H) - \rho(0))/\rho(0) \times 100$ increases dramatically before becoming linear, as shown in Fig. 3(b). With increasing temperature, the region of linearity is suppressed, as well as the magnitude of the sudden upturn in MR. This sudden upturn in MR has been observed in other systems and can be explained by quantum interference effects such as weak localization or weak antilocalization, the latter of which has often been observed in the 2D Dirac surface states of topological insulators and in 3D Dirac semimetal thin films.[34–37] Furthermore, linear magnetoresistance has been known to arise in topological systems, and its presence in $LaCuSb_2$ further gives evidence for the presence of Dirac fermions in this system. Hall measurements of $LaCuSb_2$ indicate that the dominant carriers are

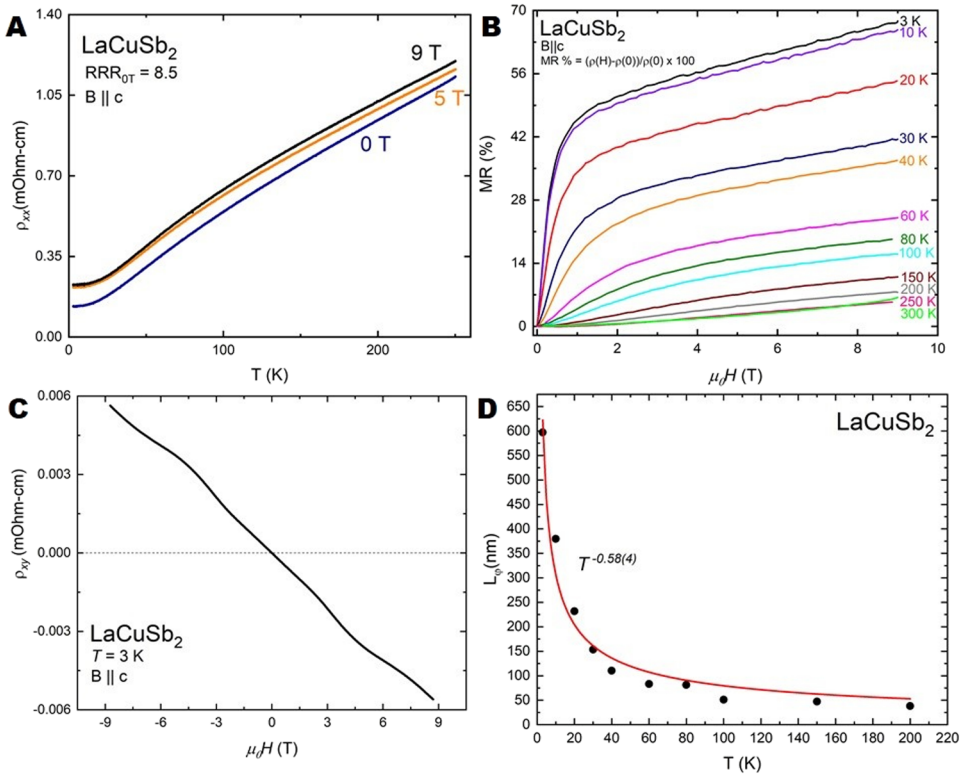

FIG. 3. (a) The resistivity as a function of temperature indicates metallic behavior and generally increases upon applying magnetic fields at all temperatures. The RRR of 8.5 indicates that the sample is of high quality. (b) The magnetoresistance of $LaCuSb_2$ increases dramatically up to around ~2 T at the lowest measured temperature of T = 3 K, after which the dependence becomes linear with the applied field. The region of linearity decreases with increasing temperature but is somewhat regained at all fields past 200 K. The dramatic increase in magnetoresistance at low fields and low temperatures is due to the presence of weak antilocalization in this system. (c) Measurements of the Hall effect in $LaCuSb_2$ suggest electrons to be the main carriers in this system. The nonlinearity of the curve is due to issues with data collection and symmetrization. (d) The phase coherence length of carriers in $LaCuSb_2$ as extracted by fitting the low-field magnetoresistance curves of $LaCuSb_2$ to the HLN theory for weak antilocalization. The $T^{-0.58(4)}$ power law dependence of L_φ with temperature indicates that the weak antilocalization is two-dimensional.

electrons, given the negative slope of R_{xy}, with a relatively high carrier concentration of 2.74×10^{18} cm^{-3} at 3 K, as shown in Fig. 3(c). This value requires a consideration of a large Hall angle, given the large difference in ρ_{xx} vs ρ_{xy}, and complicates symmetrization of the data, resulting in apparent nonlinearity. This is likely due to the presence of other bands at the Fermi level, which act to enlarge the Fermi surface from that expected for a simple Dirac system. Further studies are required to investigate whether the Hall behavior is intrinsically linear or not.

As aforementioned, a large upturn is observed in the magnetoresistance of $LaCuSb_2$, especially at low temperatures. This upturn can be ascribed to weak antilocalization, a phenomenon that occurs in the quantum diffusive regime of metallic materials, whereby the electron phase coherence lengths are longer than the electron mean free path lengths. Applying a magnetic field and consequently breaking time reversal symmetry results in a dramatic decrease in conductivity with small applied fields or a converse increase in resistivity, i.e., what is observed in our magnetoresistance data. Weak antilocalization has been observed in many topological materials harboring Dirac fermions because of the π Berry phase picked up after circulating around the Fermi surface. This π Berry phase then generates destructive quantum interference that can suppress backscattering and lead to an increase in conductivity with decreasing temperature. However, applying a magnetic field and breaking time-reversal symmetry negates this effect and results in a large decrease in the conductivity with small applied fields.

Based on Hikami-Larkin-Nagaoka (HLN) theory, the weak antilocalization in $LaCuSb_2$ can be understood by fitting the magnetoconductivity to the following equation:

$$\Delta\sigma(B) = \frac{\alpha e^2}{2\pi^2\hbar}\left[\psi\left(\frac{1}{2}+\frac{\hbar}{4eBL_\varphi^2}\right) - \ln\left(\frac{\hbar}{4eBL_\varphi^2}\right)\right],$$

where $\alpha = -\frac{1}{2}$ due to the π Berry phase, ψ is the Digamma function, and L_φ is the phase coherence length. The temperature dependence of L_φ can be seen in Fig. 3(d). It follows a $T^{-0.58(4)}$ law, which is very close to the $T^{-0.5}$ relation expected for a two-dimensional system.[34] This indicates that the weak antilocalization in this material is two-dimensional, which may be due to the dimensionality of the Sb square-lattice. However, weak antilocalization in bulk materials is uncommon and has only been observed in a very small number of bulk materials. Weak antilocalization effects are more commonly observed in topological insulator films due to the pronounced effect of the Dirac surface states due to the thinness of the samples.[35–37] An alternative explanation, based on a two-band model, can be found in the supplementary material.

In $LaCuSb_2$, periodic SdH quantum oscillations in the resistivity at high magnetic fields can be observed, as shown in Fig. 4(a) for T = 0.27 K as a function of inverse field. The single crystal structure, patterned by focused-ion-beam lithography, used to measure these is shown in Fig. 4(b). These oscillations are due to the cyclotron motion of carriers on the Fermi surface. Performing a Fast Fourier Transform (FFT) operation on SdH data collected at temperatures

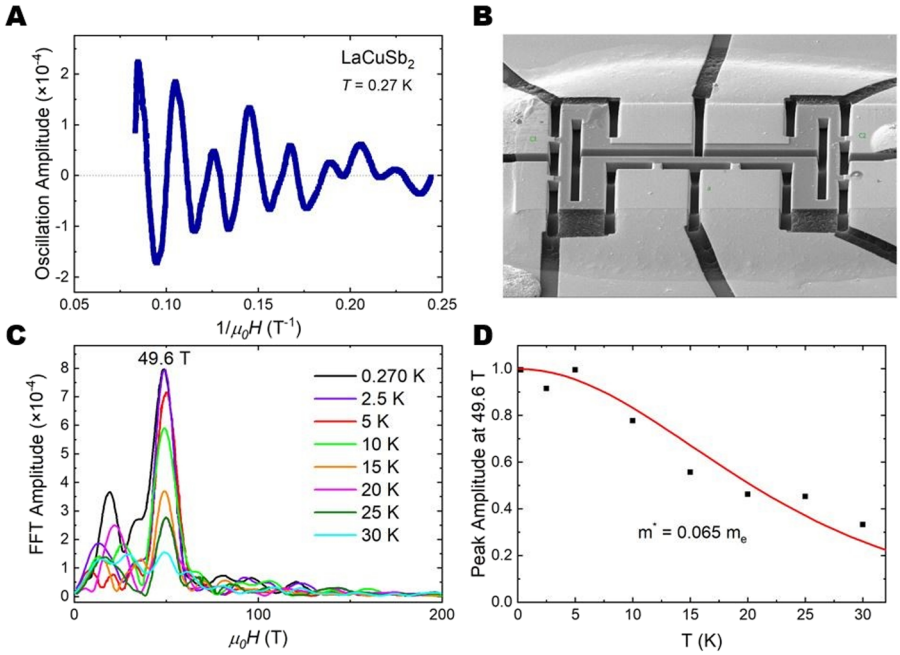

FIG. 4. (a) Oscillation amplitude as a function of inverse field at T = 0.27 K for $LaCuSb_2$ demonstrates large oscillations at high fields. (b) A scanning electron microscopy image of the focused-ion beam cut device of $LaCuSb_2$ used for SdH oscillations measurements. (c) Plot showing the Fast Fourier Transform (FFT) of the SdH oscillations at eight different temperatures. While several frequency amplitudes are observed, a frequency peak at 49.6 T is observed at all temperatures. (d) The evolution of the 49.6 T frequency peak, shown in (c), with temperature. A fit to Lifshitz-Kosevich theory yields an effective mass of 6.5% the electron rest mass.

up to T = 30 K reveals the amplitudes of dominant frequencies of oscillation, as shown in Fig. 4(c). The main frequency of oscillation is observed to be 49.6 T. Finally, by considering the temperature dependence of the 49.6 T FFT amplitude shown in Fig. 4(c), the effective carrier mass m^* can be obtained by fitting to the Lifshitz-Kosevich theory, as shown in Fig. 4(d).[38] This value was found to be $m^* = 0.065m_e$, where m_e is the electron rest mass. Through the oscillation frequency, we determine the Fermi momentum k_F to be equal to 3.88×10^8 m^{-1}. By considering the Onsager relation for the carrier concentration of $n = [2/(2\pi)^3](4\pi/3k_F^3)$, we obtain $n = 1.97 \times 10^{18}$ cm^{-3}, which is in agreement with the Hall measurement result. It should be noted that this applies to an isotropic three-dimensional pocket and not to a two-dimensional one, and thus, $LaCuSb_2$ appears to display more three-dimensional behavior than other 112 systems. The ultralow carrier mass obtained is found to be smaller than that for other 112 Dirac systems[16–27] and is generally lower than one would expect for conventional (non-Dirac) carriers. These observations provide strong evidence for the presence of Dirac fermions in $LaCuSb_2$.

Our results show strong evidence for the presence of Dirac fermions in $LaCuSb_2$. In addition to this observation, there have been potentially interesting claims of intrinsic superconductivity in this system in the literature, under T = 0.9 K,[39,40] which in the context of our discovery may present an interesting example of a material at the interface of superconductivity and topology.[41] Our measurements, however, of both resistivity and specific heat in multiple samples down to temperatures far below T = 0.9 K have shown no anomaly consistent with a superconducting phase transition. Subsequent studies could vary the synthesis techniques and search for superconductivity in this interesting system.

EXPERIMENTAL

Centimeter-sized single crystals of $LaCuSb_2$ were grown by the flux method using antimony.[42] Stoichiometric amounts of La (99.99%) and Cu (99.99%) were placed in an alumina crucible, and Sb (99.999%) was added in thirtyfold molar excess as both reagent and flux. The crucible was placed inside a sealed fused silica tube under vacuum, and the reaction was stepped to 1050 °C, soaked for 12 h, and then cooled slowly to 650 °C at a rate of 5 °C/h. The reaction vessel was then centrifuged to remove excess Sb flux. Large crystals, limited mainly in size by the crucible, can be obtained. The crystals are visibly layered and easy to cut and handle, and are air and moisture stable.

Representative crystals were ground, and their crystal structure was determined using X-ray diffraction on a laboratory Bruker D8 Focus diffractometer (Cu tube, $K\alpha_1$: 1.540 596 Å and $K\alpha_2$: 1.544 493 Å) with a LynxEye detector. The structure was found to be consistent with stoichiometric $LaCuSb_2$ based on previous structural studies of this material.[28,33]

Electronic transport and heat capacity data were collected on crystals in a Quantum Design physical property measurement system. Resistivity measurements used standard four probe geometry on a bar shaped cut crystal, whereas Hall measurements were performed using a crystal cut in the shape of a square, with leads attached in the proper Hall geometry. Angular dependent transport data were collected using the Quantum Design horizontal rotator option. Heat capacity measurements were performed under T = 3 K using a Quantum Design dilution refrigerator.

Electronic and band structure calculations were performed on $LaCuSb_2$ by means of DFT with the local density approximation (LDA), using the Elk all-electron full-potential linearized

augmented-plane wave plus local orbitals (FP-LAPW + LO) code.[43] Calculations were performed both with and without SOC using an $8 \times 8 \times 8$ k-point mesh.

ARPES spectra were recorded on the UE112-PGM2a beamline at Bessy II in Berlin, Germany. The utilized 1^2 endstation is equipped with a Scienta R8000 detector. Samples were cleaved *in situ* in ultra-high vacuum (low 10^{-10} mbar pressure range) and measured at a temperature of 40 K.

Measurements of SdH oscillations were performed on a single-crystal structure prepared using focused ion beam lithography. Four-point resistance measurements of the c-axis resistivity were made using an excitation current of 150 μA, with magnetic fields up to 12 T applied along the c-axis, at temperatures between $T = 0.27$ and 30 K.

SUPPLEMENTAL MATERIAL

See the supplementary material for a more in-depth discussion of the ARPES findings and a discussion of other possible sources of linear magnetoresistance in this material.

ACKNOWLEDGMENTS

This work was supported as part of the Institute for Quantum Matter, an Energy Frontier Research Center funded by the U.S. Department of Energy, Office of Science, Office of Basic Energy Sciences, under Award No. DE-SC0019331. L.M.S. was supported by NSF through the Princeton Center for Complex Materials, a Materials Research Science and Engineering Center (Grant No. DMR-1420541), and by a MURI grant on Topological Insulators from the Army Research Office (Grant No. ARO W911NF-12-1-0461). A.T. was supported by the DFG (Proposal No. SCHO 1730/1-1). Y.F. and B.J.R. are supported by the National Science Foundation under Grant No. 1752784. We thank HZB for the allocation of synchrotron radiation beamtime.

REFERENCES

[1] C. L. Kane and E. J. Mele, "Z(2) topological order and the quantum spin Hall effect," Phys. Rev. Lett. **95**, 146802 (2005).
[2] C. L. Kane and E. J. Mele, "Quantum spin Hall effect in graphene," Phys. Rev. Lett. **95**, 226801 (2005).
[3] M. Z. Hasan and C. L. Kane, "Colloquium: Topological insulators," Rev. Mod. Phys. **82**, 3045–3067 (2010).
[4] H. J. Zhang *et al.*, "Topological insulators in Bi_2Se_3, Bi_2Te_3 and Sb_2Te_3 with a single Dirac cone on the surface," Nat. Phys. **5**, 438–442 (2009).
[5] L. Fu, C. L. Kane, and E. J. Mele, "Topological insulators in three dimensions," Phys. Rev. Lett. **98**, 106803 (2007).
[6] Z. K. Liu *et al.*, "Discovery of a three-dimensional topological Dirac semimetal Na_3Bi," Science **343**, 864–867 (2014).
[7] T. Liang *et al.*, "Ultrahigh mobility and giant magnetoresistance in the Dirac semimetal Cd_3As_2," Nat. Mater. **14**, 280–284 (2015).
[8] B. Q. Lv *et al.*, "Experimental discovery of Weyl semimetal TaAs," Phys. Rev. X **5**, 031013 (2015).
[9] C. Fang, H. M. Weng, X. Dai, and Z. Fang, "Topological nodal line semimetals," Chin. Phys. B **25**, 117106 (2016).
[10] L. M. Schoop, F. Pielnhofer, and B. V. Lotsch, "Chemical principles of topological semimetals," Chem. Mater. **30**, 3155–3176 (2018).
[11] H. Li *et al.*, "Negative magnetoresistance in Dirac semimetal Cd_3As_2," Nat. Commun. **7**, 10301 (2016).
[12] Y. B. Zhang, Y. W. Tan, H. L. Stormer, and P. Kim, "Experimental observation of the quantum Hall effect and Berry's phase in graphene," Nature **438**, 201–204 (2005).
[13] M. Neupane *et al.*, "Observation of a three-dimensional topological Dirac semimetal phase in high-mobility Cd_3As_2," Nat. Commun. **5**, 3786 (2014).
[14] K. I. Bolotin *et al.*, "Ultrahigh electron mobility in suspended graphene," Solid State Commun. **146**, 351–355 (2008).
[15] K. S. Novoselov *et al.*, "Two-dimensional gas of massless Dirac fermions in graphene," Nature **438**, 197–200 (2005).
[16] J. B. He *et al.*, "Quasi-two-dimensional massless Dirac fermions in $CaMnSb_2$," Phys. Rev. B **95**, 045128 (2017).
[17] Y. Feng *et al.*, "Strong anisotropy of Dirac cones in $SrMnBi_2$ and $CaMnBi_2$ revealed by angle-resolved photoemission spectroscopy," Sci. Rep. **4**, 5385 (2014).
[18] A. M. Zhang *et al.*, "Interplay of Dirac electrons and magnetism in $CaMnBi_2$ and $SrMnBi_2$," Nat. Commun. **7**, 13833 (2016).
[19] J. Y. Liu *et al.*, "A magnetic topological semimetal $Sr_{1-y}Mn_{1-z}Sb_2$ (y, z < 0.1)," Nat. Mater. **16**, 905 (2017).
[20] J. Y. Liu *et al.*, "Nearly massless Dirac fermions hosted by Sb square net in $BaMnSb_2$," Sci. Rep. **6**, 30525 (2016).
[21] S. L. Huang, J. Kim, W. A. Shelton, E. W. Plummer, and R. Y. Jin, "Nontrivial Berry phase in magnetic $BaMnSb_2$ semimetal," Proc. Natl. Acad. Sci. U. S. A. **114**, 6256–6261 (2017).
[22] H. Masuda *et al.*, "Quantum Hall effect in a bulk antiferromagnet $EuMnBi_2$ with magnetically confined two-dimensional Dirac fermions," Sci. Adv. **2**, e1501117 (2016).
[23] Y. Y. Wang, S. Xu, L. L. Sun, and T. L. Xia, "Quantum oscillations and coherent interlayer transport in a new topological Dirac semimetal candidate $YbMnSb_2$," Phys. Rev. Mater. **2**, 021201 (2018).
[24] J. Y. Liu *et al.*, "Unusual interlayer quantum transport behavior caused by the zeroth Landau level in $YbMnBi_2$," Nat. Commun. **8**, 646 (2017).
[25] K. F. Wang, D. Graf, and C. Petrovic, "Quasi-two-dimensional Dirac fermions and quantum magnetoresistance in $LaAgBi_2$," Phys. Rev. B **87**, 235101 (2013).
[26] K. F. Wang and C. Petrovic, "Multiband effects and possible Dirac states in $LaAgSb_2$," Phys. Rev. B **86**, 155213 (2012).
[27] X. Shi *et al.*, "Observation of Dirac-like band dispersion in $LaAgSb_2$," Phys. Rev. B **93**, 081105 (2016).
[28] X. X. Yang *et al.*, "$RCu_{1+x}Sb_2$ (R = La, Ce, Pr, Nd, Sm, Gd, Tb, Dy, Ho and Y) phases with defect $CaBe_2Ge_2$-type structure," Mater. Sci. Forum **475-479**, 861–864 (2005).
[29] W. Tremel and R. Hoffmann, "Square nets of main group elements in solid-state materials," J. Am. Chem. Soc. **109**, 124–140 (1987).
[30] S. Klemenz, S. Lei, and L. M. Schoop, "Topological semimetals in square-net materials," Annu. Rev. Mater. Res. **49**(1), 185–206 (2019).
[31] L. M. Schoop *et al.*, "Dirac cone protected by non-symmorphic symmetry and three-dimensional Dirac line node in ZrSiS," Nat. Commun. **7**, 11696 (2016).
[32] A. Topp *et al.*, "Non-symmorphic band degeneracy at the fermi level in ZrSiTe," New J. Phys. **18**, 125014 (2016).
[33] O. Sologub, K. Hiebl, P. Rogl, H. Noel, and O. Bodak, "On the crystal-structure and magnetic-properties of the ternary rare-earth compounds $RETSb_2$ with Re-equivalent-to-rare earth and T-equivalent-to-Ni, Pd, Cu and Au," J. Alloys Compd. **210**, 153–157 (1994).
[34] B. L. Altshuler, A. G. Aronov, and D. E. Khmelnitsky, "Effects of electron-electron collisions with small energy transfers on quantum localization," J. Alloys Compd. **15**, 7367–7386 (1982).
[35] R. K. Gopal, S. Singh, R. Chandra, and C. Mitra, "Weak-antilocalization and surface dominated transport in topological insulator Bi_2Se_2Te," AIP Adv. **5**, 047111 (2015).
[36] L. H. Bao *et al.*, "Weak anti-localization and quantum oscillations of surface states in topological insulator Bi_2Se_2Te," Sci. Rep. **2**, 726 (2012).
[37] Y. S. Kim *et al.*, "Thickness-dependent bulk properties and weak antilocalization effect in topological insulator Bi_2Se_3," Phys. Rev. B **84**, 073109 (2011).
[38] E. M. Lifshits and A. M. Kosevich, "Theory of the Shubnikov-Dehaas effect," J. Phys. Chem. Solids **4**, 1–10 (1958).

[39]K. V. Lakshmi, L. Menon, A. K. Nigam, A. Das, and S. K. Malik, "Magnetoresistance studies on $RTSb_2$ compounds (R = La, Ce and T = Ni, Cu)," Physica B **223-24**, 289–291 (1996).
[40]N. V. Gamayunova *et al.*, "Electron-phonon interaction in ternary rare-earth copper antimonides $LaCuSb_2$ and $La(Cu_{0.8}Ag_{0.2})Sb_2$ probed by Yanson point-contact spectroscopy," in *2017 IEEE 7th International Conference Nanomaterials: Application and Properties (NAP)* (IEEE, 2017).
[41]P. Ruszala, M. J. Winiarski, and M. Samsel-Czekala, "Dirac-like band structure of $LaTESb_2$ (TE = Ni, Cu, and Pd) superconductors by DFT calculations," Comput. Mater. Sci. **154**, 106–110 (2018).
[42]P. C. Canfield and Z. Fisk, "Growth of single-crystals from metallic fluxes," Philos. Mag. B **65**, 1117–1123 (1992).
[43]A. A. Mostofi *et al.*, "Wannier90: A tool for obtaining maximally-localised Wannier functions," Comput. Phys. Commun. **178**, 685–699 (2008).